

# Evaluation of mechanical properties of Ni/BaTiO<sub>3</sub> functionally graded material

Baraa Saidani<sup>1</sup>, Jihed Zghal<sup>1,\*</sup>, Isabelle Bruant<sup>1,\*\*</sup>, Damien Bregiroux<sup>2</sup>, Johann Petit<sup>1</sup>, Julie Cedelle<sup>1</sup>, and Gaël Chevallier<sup>\*\*\*</sup>

<sup>1</sup> Laboratoire Energétique Mécanique Electromagnétisme (LEME),

<sup>2</sup> Sorbonne Université, CNRS, Chimie de la Matière Condensée de Paris, LCMCP, Paris, 75005 France

<sup>3</sup> Franche-Comté Electronics Mechanics Thermal Science and Optics – Sciences and Technologies (FEMTO-ST),

Received: 6 June 2023 / Accepted: 15 November 2023

**Abstract.** A Ni-BaTiO<sub>3</sub> functionally graded material (FGM) was elaborated from 5 separate layers, ranging from 0 to 100 wt.% Ni content, by Spark Plasma Sintering (SPS) method. To estimate the variation of mechanical properties in the FGM thickness, 5 homogenous mixtures (100% BaTiO<sub>3</sub>, 75% BaTiO<sub>3</sub>-25% Ni, 50% BaTiO<sub>3</sub> - 50% Ni, 25% BaTiO<sub>3</sub>-75% Ni and 100% Ni) were sintered. The density, the Vickers hardness, the Young's modulus and Poisson ratio were measured. In order to observe the impact of polarization on their properties (in future work), non-destructive tests are performed in this study. Results from monolithic pellet are gathered to identify the power law that governs the variation of this property in the FGM thickness. The results show that each property has its own power law.

**Keywords:** FGM materials / mechanical characterization / power law / Spark Plasma Sintering (SPS)

## 1 Introduction

During the last decades, extensive research on active vibration control and energy harvesting has been carried out using piezoelectric materials. Recently, a new class of the well-known functionally graded materials (FGM) mixing metal and ceramic piezoelectric in a single material, has attracted much attention for these applications. They are defined as functionally graded piezoelectric material (FGPM) and are designed to achieve functional features such as structural damping, with mechanical and piezoelectric properties that gradually evolve along one direction. This ideal/perfect continuity in properties variation allows to avoid the disadvantages of classical smart structures, in particular the interface problem issues between the structure and the piezoelectric actuator. As a result, they offer better specific strength, toughness and fatigue resistance than classical composite materials, making them appropriate for transducers use [1]. Numerical simulations showed their effectiveness in active vibration control [2–4] and energy harvesting [5,6].

However, very few experimental works deal with their elaboration. To the best of the authors' knowledge, their effective properties are not well known, in particular, the variation of the properties in the FGM direction. Therefore, the objective of this study is the elaboration of an FGM metallic/piezoceramic sample and the evaluation of mechanical properties (the characterization of piezoelectric properties will be considered in a next step).

Several papers deal with the elaboration of samples made from two different powders (usually ceramic and metallic). Under the European REACH regulation, the use of lead in piezoelectric ceramics is gradually being banned to protect the health of living beings and the environment. Piezoelectric composite polymers based on BaTiO<sub>3</sub> piezoceramics possess high piezoelectric coefficients and are nontoxic. First BaTiO<sub>3</sub>/Ni composites were fabricated by Emoto [7] and Pecharrroman [8] considering 0 to 40 wt.% of Ni. In [9], BaTiO<sub>3</sub>/Ni composites were prepared from 0 to 23 wt.%. In these papers, the dielectric properties were characterized. Barium titanate-silver composites were manufactured with silver contents ranging from 0 to 30 wt.% in [10]. BaTiO<sub>3</sub>/Cu composite ceramics were fabricated in [11], considering 0 to 30 wt.% of Cu. The influence of adsorbed moisture on the properties of cyanate ester/BaTiO<sub>3</sub> composites has been studied by Chao [12]. In all these studies, the samples were made with conventional

\* e-mail: [jihed.zghal@parisnanterre.fr](mailto:jihed.zghal@parisnanterre.fr);

\*\* e-mail: [isabelle.bruant@parisnanterre.fr](mailto:isabelle.bruant@parisnanterre.fr);

\*\*\* e-mail: [gael.chevallier@univ-fcomte.fr](mailto:gael.chevallier@univ-fcomte.fr).

sintering. Watanabe [13] deals with the Spark Plasma Sintering (SPS) of SiC/graphite functionally graded materials. The structure contains 5 layers from 0 to 100 wt.% SiC. In [14], several FGM Al-SiC-graphite are made up of 4 layers from 50 to 100 wt.% Al.

Few papers deal with the fabrication of FGPM, most of them dealing with lead-based piezoceramics. In [15], the fabrication of PZT/Pt FGM bimorph actuator was considered. It consists on 7 layers with a center-symmetric composition profile, in which the compositions from the central layer to the surface layer were stepwise changed from 30 to 0% wt. Pt in an interval of 10%. The electrically induced bending displacement was measured. A functionally graded PZT/Ag actuator was elaborated by Zhang [16]. It is made with 3 layers from 0 to 15 wt.% Ag. In [1], BTO/PVDF FGPM composites were manufactured, made with 6 layers from 0 to 50 wt. % BTO. The material energy harvesting potential was investigated. In these previous papers, the samples were made with conventional sintering technology.

The mechanical properties in these papers were rarely evaluated. Typically, there are two approaches used to measure these properties. The first one involves destructive tests (three-point bending, tensile, compression ...) which are commonly employed. In [11], the bending strength and fracture toughness were measured by three-point bending. In contrast, the second approach allows for preserving the sample's integrity. In this case, the nanoindentation and ultrasonics methods provide information at a micro and macro levels, respectively. The characterization of mechanical properties by nanoindentation of BaTiO<sub>3</sub> ceramic with different types of sintering aid was presented in [17]. Three BaTiO<sub>3</sub> powders of various particle size distributions were considered in [18]. The effect of the grain size on the mechanical properties of the BaTiO<sub>3</sub> pellets was studied through uniaxial compression test. W/Cu FGM with 11 layers from 0 wt.% to 100 wt.% Cu were fabricated in [19]. They were characterized by performing tensile strength tests. Farahmand [20] suggested evaluating the elastic properties of Al<sub>2</sub>O<sub>3</sub>/Al FGMs by longitudinal and transverse ultrasonic bulk waves velocity features. Their pellets were made up of 5 layers from 0 to 40 wt.% Al, with SPS technic. In the same way, in [21], longitudinal elastic constants were measured using ultrasound phase spectroscopy of Al-SiC-graphite FGMs.

These articles show that the elaboration of FGPM is quite difficult. The strong difference between metal and ceramic thermal expansion coefficient leads to important stresses and microcracks at the interfaces. Moreover, it is important to avoid all chemical reactions between the two materials during the high temperature sintering step. Metals and ceramics generally have very different sintering temperatures. For instance, BaTiO<sub>3</sub> is sintered in the range 1200 – 1300 °C for several hours [22]. Innovative processing methods, including SPS [23], allow to decrease the sintering temperature up to approximately 900 °C and to achieve a full densification in only few minutes [24– 26]. Metal with a melting point higher than the ceramic sintering temperature, i.e., 900 °C, is required. The Ni sintering temperature being closed to that of BaTiO<sub>3</sub>, the present study focuses on FGM made from Ni and BaTiO<sub>3</sub> powders. These FGM

**Table 1.** Composition of each layer of Ni/ BaTiO<sub>3</sub> FGM.

Layer number	Composition of each layer
1	100% BaTiO <sub>3</sub>
2	25% Ni + 75% BaTiO <sub>3</sub>
3	50% Ni + 50% BaTiO <sub>3</sub>
4	75% Ni + 25% BaTiO <sub>3</sub>
5	100% Ni

samples were elaborated by SPS, by co-sintering five BaTiO<sub>3</sub>/Ni powder mixture layers with compositions gradually ranging from 0 to 100 vol % Ni in the thickness of the samples. Physical (density) and mechanical properties (Vickers hardness, Young's modulus and Poisson ratio) were measured. The small size of the pellets requires adequate characterization methods for mechanical properties. The ultrasonic testing was proposed as fast, repeatable and nondestructive technique to estimate the elastic properties. This method ensures that the samples remain undamaged during the characterization procedure. Then, they will be polarized in order to observe the impact of polarization on their properties (in a future work). From these experimental results, the power law parameters modelling the properties variation, are identified using the least squares method.

The Section 2 presents the FGM manufacturing. In Section 3, the experimental procedure for the characterization of physical and mechanical properties are detailed. The variation of each property in the FGM thickness is estimated from experimental measures. Results are discussed in Section 4. The main conclusions are summarized in the last section.

## 2 FGM pellets elaboration

Three FGM Ni/ BaTiO<sub>3</sub> pellets were elaborated by SPS technique from the mixture of two powders. The first one is a commercial nano-powder of BaTiO<sub>3</sub> (Sigma-Aldrich, purity > 99%) with grain size lower to 100 nm. The second one is a Ni micrometric powder, with average particle size of 0.8 micron (Sigma-Aldrich, purity > 99.8%). The mixtures of Ni and BaTiO<sub>3</sub> powders were prepared by respecting the following evolution of the volume fraction  $V_m$  as a function of thickness  $z$  (Eq. (1)):

$$V_m(z) = \frac{z}{h}, \quad z \in [0, h], \quad (1)$$

with  $h$  the pellet thickness. Moreover, due to the experimental difficulty to have the right mixture variation, pellets were developed according to a 5-step staircase function in the thickness. As a result, the obtained FGM samples are made up of five stacked layers with different volume fraction. Table 1 lists each layer composition in the Ni/BaTiO<sub>3</sub> FGM. The five mixtures were stacked layer by layer, in a graphite die, of axis  $z$ , with a 10 mm inner

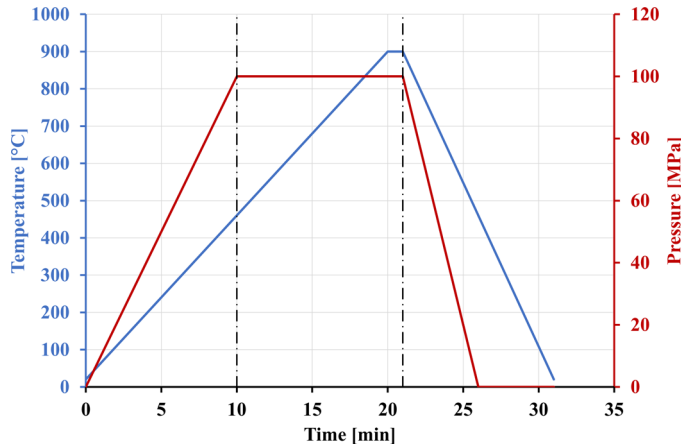


Fig. 1. Temperature and loading for SPS.

diameter and sintered in a vacuum through the SPS technique (Dr. Sinter-Lab SPS-515S, SPS Sintex Inc.). SPS sintering consists of heating the sample very quickly while applying a uniaxial pressure. Thus, it is possible to densify the material in very short time and limiting both grain growth and the interdiffusion of different chemical species. In this work, powders were sintered with a constant applied pressure of 100 MPa. The heating rate was fixed to 50 °C/min. The cooling rate was around 90 °C/min (Fig. 1). The final FGM thickness is around 3 mm.

In order to validate the elaboration process and ensure that we got high density for FGM Ni-BaTiO<sub>3</sub>, microscopic observation of the cross section was carried out (Fig. 2) using Keyence digital microscope VHX-7000. Observations show that:

- It's possible to obtain a dense material in very short time, by limiting both the grain growth and the inter-diffusion of the different chemical species.
- There is no loss of cohesion (no microcracks).
- The transitions between individual layers are viewable. The interlayer regions could be smoother by using more thinner layers. For example, instead of moving from one layer to another in the FGM in 25% increments, a smaller increment of 10% could be considered. This would allow for a more gradual and seamless transition between adjacent layers, enhancing the overall quality and structural integrity of the FGM.
- The thickness is relatively non-homogenous, especially near the edges. The average and standard deviation of the thickness of each layer are given Figure 3. The gap between each layer thickness is due to the hand-made compaction.

Complementary observations of the FGM microstructure were also conducted using a JEOL JSM-6010PLUS scanning electronic MEB (Fig. 4). They show:

- Ni-BaTiO<sub>3</sub> FGM contains some porosities. These porosities are more important in the 100% BaTiO<sub>3</sub> layer than the other ones. In the 100% BaTiO<sub>3</sub> layer material,

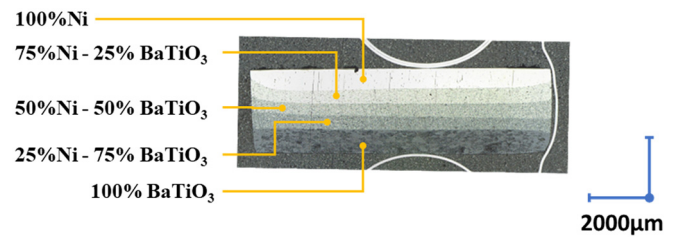


Fig. 2. Microscopic observation of Ni-BaTiO<sub>3</sub> FGM.

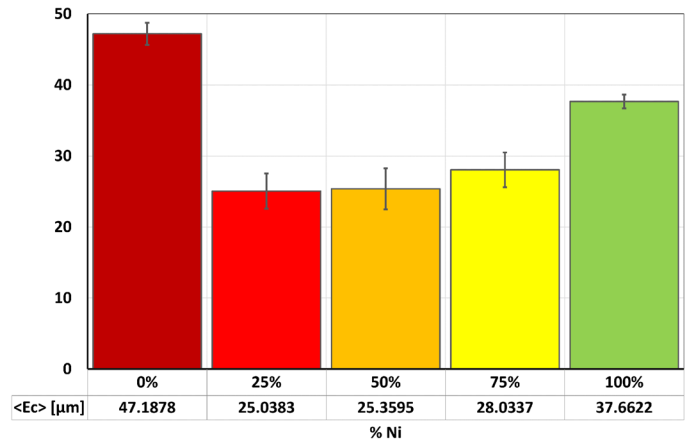


Fig. 3. Average thickness of each FGM layer.

some areas have nearly complete densification, whereas other regions still not be densified. The 100% Ni contains the lowest quantity of porosity.

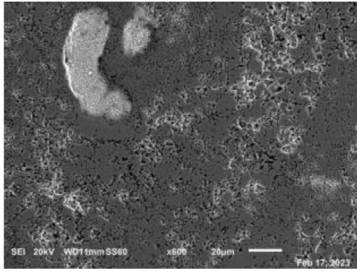
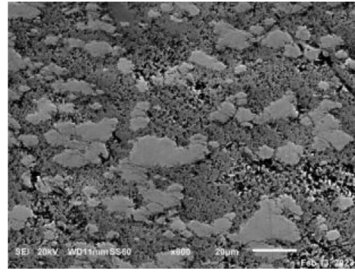
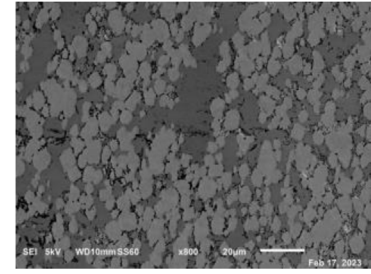
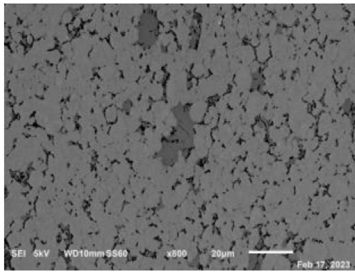
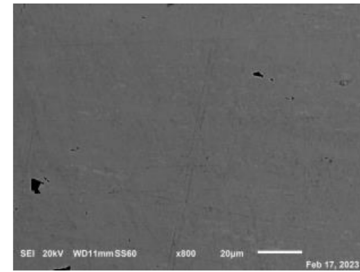
- The SPS process allows us to obtain dense material but different types of grains in the different layers can be observed. It can be explained by the temperature and loading cycle during SPS.

Based on these observations, three monolithic pellets having composition identical to the different layers of the FGM, were elaborated by SPS in order to characterize each one. To estimate the properties variation in the FGM thickness, we suppose that each monolithic pellet has the same properties of the corresponding layer in the Ni-BaTiO<sub>3</sub> FGM.

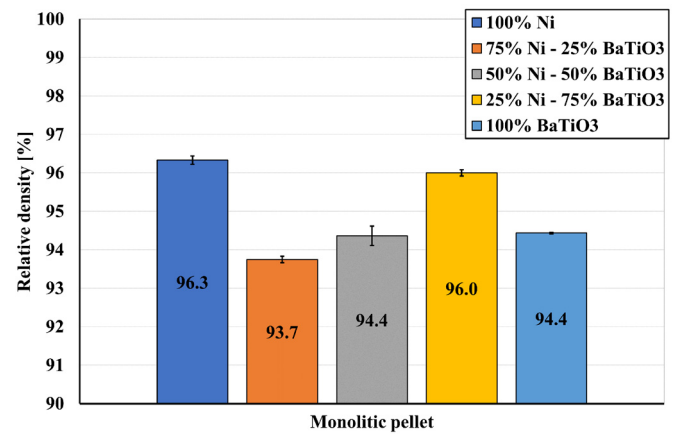
The elaborated samples are cylindrical pellets, of 10 mm diameter and 5 mm thickness (Fig. 5).

### 3 Ni-BaTiO<sub>3</sub> FGM characterization

In this section, the variation in the thickness of Density, Young's modulus, Poisson ratio and Hardness of the Ni-BaTiO<sub>3</sub> FGM is estimated. For this purpose, each of these properties are characterized on monolithic pellets. Then, by fitting these experimental data, the variation of each property in the FGM thickness is obtained from the

(a) Layer 1: 100% BaTiO<sub>3</sub>(b) Layer 2: 25% BaTiO<sub>3</sub>+75% Ni(c) Layer 3: 50% BaTiO<sub>3</sub>+50% Ni(d) Layer 4: 75% BaTiO<sub>3</sub>+25% Ni

(e) Layer 5: 100% Ni

**Fig. 4.** SEM observation of each Ni-BaTiO<sub>3</sub> FGM layer.**Fig. 5.** One monolithic pellet.**Fig. 6.** Relative density of each monolithic pellet.

power law given to equation (2):

$$P(V_m) = (P_m - P_c)V_m^k + P_c. \quad (2)$$

Here, the subscript “m” denotes metal (Nickel) and “c” ceramic (BaTiO<sub>3</sub>).

By using (Eq. (1)) in (Eq. (2)), evolution of each property of the FGM along the thickness can be expressed as:

$$P(z) = (P_m - P_c)(V_m(z))^k + P_c. \quad (3)$$

### 3.1 Density

The density of each sample was measured according to the Archimedes principle, by immersing in distilled water according to the ISO3369:2006 standard (using analysis balance Kern, Kern YDB-03 Kern & Sohn Set). First, the relative density ( $d$ ) of each pellet was calculated using:

$$d = \frac{\rho_s}{\rho_{th}} \times 100, \quad (4)$$

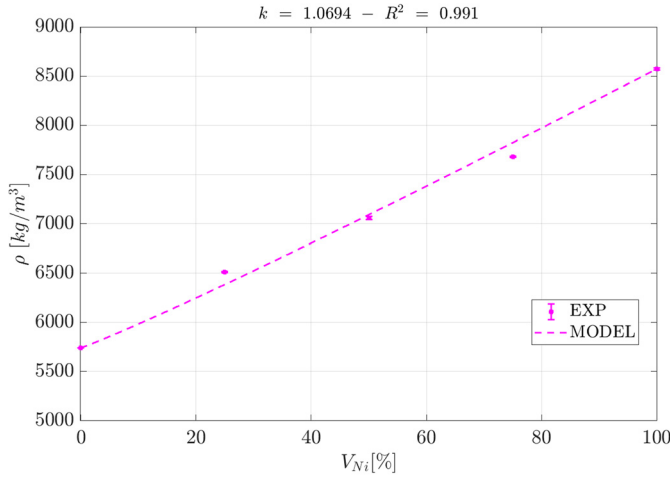


**Fig. 7.** Density variation as a function of nickel volume fraction.

where:

$\rho_s$  is the measured density of the studied pellet,

$\rho_{th}$  is the theoretical density of the studied material (Ni and BaTiO<sub>3</sub> densities were obtained from data sheets, theoretical mixtures densities were calculated using (Eq. (1)).

The relative density values of the monolithic pellets are reported in Figure 6. The gap between the different densities is small (less than 2.7%). The degree of densification obtained by SPS is fairly high (nearly 94% to 96%), suggesting presence of minor amount of residual porosity. The achieved relative density of sintered pure Ni is marginally higher compared to that of pure BaTiO<sub>3</sub>. Moreover, the relative density value of pure Ni (96%) is closed to values reported in the literature (98%) [27]. The same observation can be done for pure BaTiO<sub>3</sub> pellet: the published values are 97% [19,28] and 84.7% [29]. These findings suggest that the SPS process used in this study produced a high-density material.

Then, the density of each pellet was used to fit the power law (Eq. (4)). The identification leads to the fraction index  $k = 1.069$ , with a correlation coefficient  $R^2 = 0.991$  (Fig. 7). The standard deviation is very small, between 1.1 kg/m<sup>3</sup> and 16.4 kg/m<sup>3</sup>. Thus, the variation of the density of the Ni-BaTiO<sub>3</sub> FGM can be estimated by:

$$\rho(z) = (\rho_m - \rho_c)(V_m(z))^{1.069} + \rho_c. \quad (5)$$

### 3.2 Mechanical properties

Because of the small size of pellets, the determination of elastic properties (Young's modulus and Poisson ratio), required adequate experimental protocols that can be quite complex to set up. Furthermore, the samples had to be undamaged during the characterization procedure, since some of them would be polarized. Therefore, the classical methods (three-point bending, compression test, ...) were not useful and an ultrasonic pulse-echo technique was used. This method is well-known in the Non-Destructive Testing

(NDT) applications [30] and also in dental and civil engineering fields [31,32]. It is accurate, fast, non-destructive and applicable to small samples. Farahmand [20] and Nazeer [21] also used this technic for small FGM pellets. In this study, all monolithic pellets are considered isotropic. As both longitudinal and transverse ultrasonic wave velocities depend on the elastic properties of the material, it is possible to calculate the elastic properties of materials by measuring these wave velocities and the density. The Olympus 38DL Plus Ultrasonic Thickness Gage was used to measure velocities of Transverse  $V_T$  and the longitudinal  $V_L$  waves. Using these velocities and the density (measured previously) the Young's modulus ( $E$ ) and Poisson ratio ( $\nu$ ) of each pellet in the direction of wave propagation (over the thickness) were obtained using (Eqs. (6) and (7)).

$$\nu = \frac{1 - 2\left(\frac{V_T}{V_L}\right)^2}{2 - 2\left(\frac{V_T}{V_L}\right)^2}, \quad (6)$$

$$E = \frac{V_L^2 \rho (1 + \nu)(1 - 2\nu)}{1 - \nu} \quad (7)$$

The experimental results were fitted to identify the power law (Fig. 8). The identification shows that  $k = 0.244$  with a correlation coefficient  $R^2 = 0.977$  for the Poisson ratio and  $k = 0.874$  with a correlation coefficient  $R^2 = 0.988$  for the Young's modulus. The standard deviation is respectively, for the Poisson ratio and the Young modulus, between 0.005–0.01 and 3545 N–10492 N.

The variation of Poisson ratio and Young's modulus are then given by:

$$\nu(z) = (\nu_m - \nu_c)(V_m(z))^{0.244} + \nu_c, \quad (8)$$

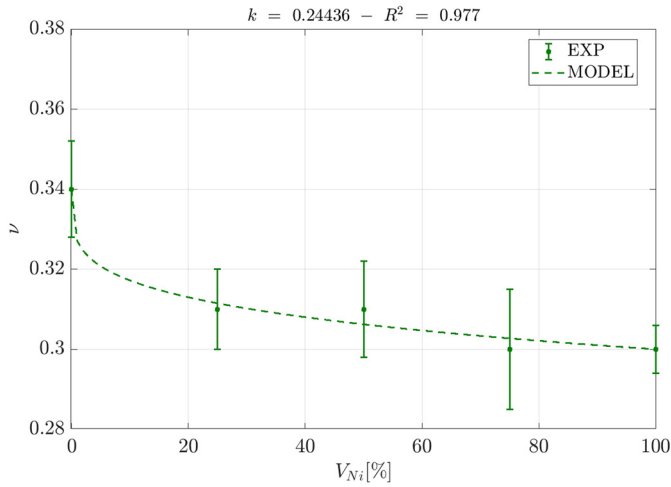
$$E(z) = (E_m - E_c)(V_m(z))^{0.874} + E_c. \quad (9)$$

### 3.3 Hardness

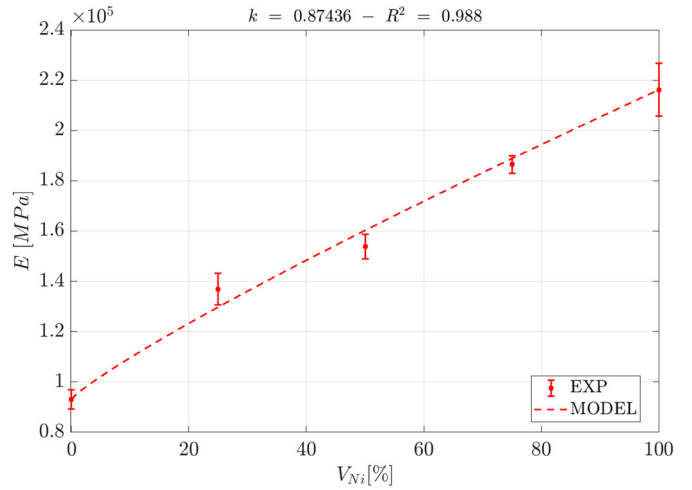
According to the ISO6507-1 standard, Vickers hardness of samples was measured using a 0.3 KgF (~2,942 N) load which allows us to undamaged the studied pellets. The hardness tester used is emco test Duravision G5. We can distinguish a large dispersion of the measured value except for pure Ni pellet (Fig. 9). The maximal standard deviation is 199 MPa. This dispersion can be explained by the heterogeneous microstructure observed in the pellets (Figs. 4a–4d), while the 100% Ni pellets present homogeneous microstructure (Fig. 4e). The values vary depending on where the measurement is taken.

The average value of hardness was fitted to identify the power law (Fig. 9). The identification leads to  $k = 0.484$  with a correlation coefficient  $R^2 = 0.782$ . The hardness variation then can be described by:

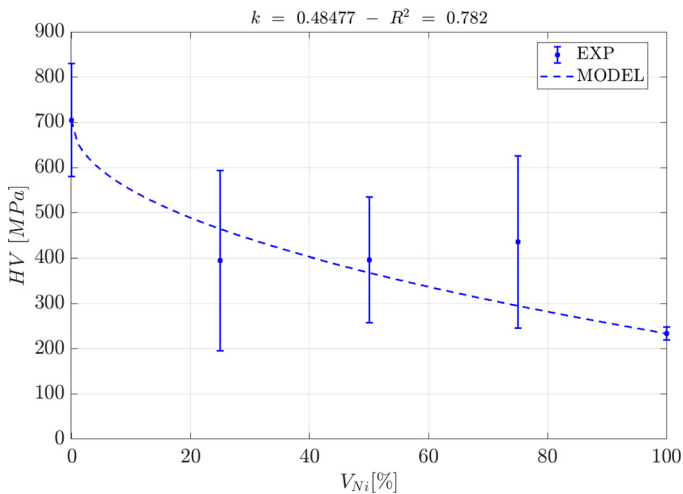
$$HV(z) = (HV_m - HV_c)(V_m(z))^{0.484} + HV_c. \quad (10)$$



(a) Poisson ratio



(b) Young's modulus

**Fig. 8.** Mechanical properties variation as a function of nickel volume fraction.**Fig. 9.** Vickers hardness variation as a function of nickel volume fraction.

Due to the wide dispersion of the measurements, these results should be considered with caution. They must be compared and validated with nanoindentation method.

## 4 Discussion

To estimate the properties variation in the FGM thickness, we have assumed here, that each monolithic pellet has the same properties of the corresponding layer in the Ni-BaTiO<sub>3</sub> FGM.

The power laws obtained for each property are summarized Table 2.

They show that:

- The index fraction of density is very closed to 1. It means that the density variation is linear in the thickness. This result is predictable because of the way that the FGM

was elaborated. The measured FGM density equals to 7390 kg/m<sup>3</sup>. It can be compared with the average value obtained from the density power law (Eq. (5)). The identification leads to the fraction index  $k=1.069$ , with a correlation coefficient  $R^2=0.991$  (Fig. 7). The results seem very closed (Tab. 3).

- The “global” Young’s modulus and Poisson ratio of the FGM pellets in the thickness direction have been measured using the pulse-echo technique. They are compared in Table 3, with the average values obtained by integrating along the thickness (i) the corresponding power laws and (ii) the expected power law with  $k=1$ . Results show that the FGM measured properties are closer to the average values obtained with the experimental index ratio than for  $k=1$ . This is a first validation that estimating the FGM properties variations from the properties measured on monolithic pellets is appropriate.
- Each physical property has its own power law. These results are in contradiction with the numerical papers like [3,5,6], which consider the same index fraction “ $k$ ” for all properties. These first results highlight the need for a better knowledge of the FGM properties in the thickness, in order to better predict the FGM behavior from numerical simulations.

## 5 Conclusion and future work

Ni-BaTiO<sub>3</sub> FGM pellets have been successfully fabricated using SPS method from BaTiO<sub>3</sub> and Ni powders, to experimentally characterize the FGM’s properties and their variation throughout the thickness direction. The interface between the adjacent layers of the sintered specimens showed no apparent defects (as gaps and delamination). Monolithic composites have also been elaborated. Physical (density) and mechanical properties (Vickers Hardness, Young’s modulus and Poisson ratio)

**Table 2.**  $k$  coefficient of the Ni-BaTiO<sub>3</sub> FGM power law.

Physical properties		$k$	$R^2$
Density	$\rho$	1.0694	0.991
Poisson ratio	$\nu$	0.24436	0.977
Young's modulus	$E$	0.87436	0.988
Hardness	$HV$	0.48477	0.782

**Table 3.** FGM physical and mechanical properties: comparison with the average values (relative error with measured value).

FGM physical properties	Measured value	Average value with $k = 1$	Average value with experimental power law
Density	7390	7112 (3.8%)	7072 (4.3%)
Poisson ratio	0.3	0.32 (6.6%)	0.308 (2.6%)
Young's modulus	168.9	154.5 (8.5%)	158.6 (6.1%)

have been measured for these samples. Since some of them will be polarized to become FGPM, the ultrasonic testing is proposed as fast, repeatable and nondestructive technique to estimate the elastic properties. From these experimental results, the variations of properties in the thickness are depicted by a classical power law. The results show that each property has its specific power law, which has not been considered so far by most authors working on the numerical modelling of the behavior of these FGPM materials.

This work highlights the need for a better understanding of the FGPM behavior to better model the active control and energy harvesting. A local identification such as the nanoindentation method will be useful to measure the elastic properties directly on the FGM. This study will allow to confirm the results obtained here and to have a more suitable results for Hardness. It will be complementary as it will provide accurate and local information on the whole thickness. At last, the next step will be the polarization of FGPM and the measure of piezoelectric properties on the same samples. It will allow us to identify if the polarization has an impact on mechanical properties.

#### Acknowledgement

We acknowledge UFR-SITEC for the generous support given to the project.

#### Funding

This research received no external funding.

#### Conflict of interest

The authors declare no conflict of interest.

#### Data availability statement

The datasets generated during and/or analysed during the current study are available from the corresponding author on reasonable request.

#### Author contribution statement

Conceptualization: B. Saidani, I. Bruant, J. Zghal, Methodology: B. Saidani, I. Bruant, J. Zghal, D. Bregiroux, J. Petit, J. Cedelle, Investigation: G. Chevalier, J. Petit, J. Cedelle, Ressources: I. Bruant, J. Zghal, D. Bregiroux, G. Chevalier, Writing—original draft preparation: B. Saidani, I. Bruant, J. Zghal, Writing—review and editing: I. Bruant, J. Zghal, G. Chevalier, Supervision: I. Bruant, J. Zghal.

#### References

- [1] Z. Wang, K. Maruyama, F. Narita, A novel manufacturing method and structural design of functionally graded piezoelectric composites for energy-harvesting, *Mater. Des.* **214**, (2022)
- [2] J. Maruani, *Contrôle Actif des Vibrations de Structures Elancées FGPM*, Thèse de doctorat, Université Paris Nanterre, Paris, 2019
- [3] J. Maruani, I. Bruant, F. Pablo, L. Gallimard, Active vibration control of a smart functionally graded piezoelectric material plate using an adaptive fuzzy controller strategy, *J. Intell. Mater. Syst. Struct.* **30**, 2065–2078 (2019)
- [4] J. Li, Y. Xue, F. Li, Y. Narita, Active vibration control of functionally graded piezoelectric material plate, *Compos. Struct.* **207**, 509–518 (2019)
- [5] Y. Cao, H. Huang, Z.H. Zhu, S. Su, Optimized energy harvesting through piezoelectric functionally graded cantilever beams, *Smart Mater. Struct.* **28**, (2019)
- [6] Y. Amini, P. Fatehi, M. Heshmati, H. Parandvar, Time domain and frequency domain analysis of functionally graded piezoelectric harvesters subjected to random vibration: finite element modeling, *Compos. Struct.* **136**, 384–393 (2016)
- [7] H. Emoto, J. Hojo, Sintering and dielectric properties of BaTiO<sub>3</sub>-Ni composite ceramics, *J. Cer. Soc. Japan*, **100**, 555–559 (1992)
- [8] C. Pecharromás, F. Esteban-Betegón, J.F. Bartolomé, S. López-Esteban, J.S. Moya, New percolative BaTiO<sub>3</sub>-Ni composites with a high and frequency-independent dielectric constant ( $\epsilon_r \approx 80000$ ), *Adv. Mater.* **13**, 1541–1544 (2021)
- [9] M. Saleem, I.S. Kim, J.S. Song, S.J. Jeong, M.S. Kim, S. Yoon, Synthesis, sintering and dielectric properties of a BaTiO<sub>3</sub>-Ni composite, *Ceram. Int.*, **40**, 7329–7335 (2014)
- [10] S. Panteny, C.R. Bowen, R. Stevens, Characterisation of barium titanate-silver composites, part I: Microstructure and mechanical properties, *J. Mater. Sci.* **41**, 3837–3843 (2006)

- [11] X. Ning, P. Yongping, W. Bo, W. Haidong, C. Kai, Enhanced mechanical and dielectric behavior of BaTiO<sub>3</sub>/Cu composites, *Ceram. Int.* **38**, 141–146 (2012)
- [12] F. Chao, N. Bowler, X. Tan, G. Liang, M.R. Kessler, Influence of adsorbed moisture on the properties of cyanate ester/BaTiO<sub>3</sub> composites, *Compos. Part A Appl. Sci. Manuf.* **40**, 1266–1271 (2009)
- [13] M. Watanabe, K. Yokoyama, Y. Imai, S. Ueta, X.L. Yan, Spark plasma sintering of SiC/graphite functionally graded materials, *Ceram. Int.* **48**, 8706–8708 (2022)
- [14] M.J. Oza, K.G. Schell, E.C. Bucharsky, T. Laha, S. Roy, Developing a hybrid Al–SiC–graphite functionally graded composite material for optimum composition and mechanical properties, *Mater. Sci. Eng. A*, **805**, (2021)
- [15] K. Takagi, J.-F. Li, S. Yokoyama, R. Watanabe, Fabrication and evaluation of PZT/Pt piezoelectric composites and functionally graded actuators, *J. Eur. Cer. Soc.*, **23**, 1577–1583 (2023)
- [16] H.L. Zhang, J.F. Li, B.P. Zhang, Fabrication and evaluation of PZT/Ag composites and functionally graded piezoelectric actuators, *J. Electroceramics*, **16**, 413–417 (2006)
- [17] S.-S. Ryu, H.-T. Kim, J. Kim, S. Kim, Characterization of mechanical properties of BaTiO<sub>3</sub> ceramic with different types of sintering aid by nanoindentation, *J. Cer. Soc. Japan*, **117**, 811–814 (2009)
- [18] T. Trzepieciniski, M. Gromada, Characterization of mechanical properties of barium titanate ceramics with different grain sizes, *Mater. Sci. Pol.* **36**, 151–156 (2018)
- [19] A. Yusefi, N. Parvin, H. Mohammadi, W–Cu functionally graded material: Low temperature fabrication and mechanical characterization, *J. Phys. Chem. Solids*, **115**, 26–35 (2018)
- [20] S. Farahmand, M.H. Soorgee, A.H. Monazzah, Evaluating the elastic properties of Al<sub>2</sub>O<sub>3</sub>–Al FGMs by longitudinal and transverse ultrasonic bulk waves velocity features, *Ceram. Int.* **47**, 24906–24915 (2021)
- [21] M. Nazeer, P. Jana, M.J. Oza, K.G. Schell, E.C. Bucharsky, T. Laha, S. Roy, Ultrasonic study of the elastic properties of functionally graded and equivalent monolithic composites, *Mater. Lett.* **323** (2022)
- [22] T. Hoshina, Y. Kigoshi, T. Furuta, H. Takeda, T. Tsurumi, Shrinkage behaviors and sintering mechanism of BaTiO<sub>3</sub> ceramics in two-step sintering, *Jpn. J. Appl. Phys.* **50** (2011)
- [23] R. Orrù, R. Licheri, A.M. Locci, A. Cincotti, G. Cao, Consolidation/synthesis of materials by electric current activated/assisted sintering, *Mater. Sci. Eng. R: Rep.* **63**, 127–287 (2009)
- [24] B. Li, X. Wang, M. Cai, L. Hao, L. Li, Densification of uniformly small-grained BaTiO<sub>3</sub> using spark-plasma-sintering, *Mater. Chem. Phys.* **82**, 173–180 (2003)
- [25] D. Bregiroux, J. Cedelle, I. Ranc, C. Barreteau, G. Mata Osoro, G. Wallez, Effect of the sintering method on microstructure and thermal and mechanical properties of zirconium oxophosphate ceramics Zr<sub>2</sub>O(PO<sub>4</sub>)<sub>2</sub>, *J. Phys. Chem. Solids*, **111**, 304–310 (2017)
- [26] H. Wang, Z. Lu, Z. Huang, J. Cedelle, Q. Wang, Size effect on hardness for micro-sized and nano-sized YAG transparent ceramics, *Ceram. Int.* **44**, 12472–12476 (2018)
- [27] G. Walunj, A. Bearden, A. Patil, T. Larimian, J. Christudasjustus, R.K. Gupta, T. Borkar, Mechanical and tribological behavior of mechanically alloyed Ni–TiC composites processed via spark plasma sintering, *Materials (Basel)*. **13**, 1–19 (2020)
- [28] W. Luan, L. Gao, H. Kawaoka, T. Sekino, K. Niihara, Fabrication and characteristics of fine-grained BaTiO<sub>3</sub> ceramics by spark plasma sintering, *Ceram. Int.* **30**, 405–410 (2004)
- [29] M.S. Jamil, K.E. Saputro, A. Noviyanto, W.B. Widayatno, A.S. Wismogroho, M.I. Amal, N.T. Rochman, T. Nishimura, Dense and fine-grained barium titanate prepared by spark plasma sintering, *J. Phys.: Conf. Ser.* **1191** (2019)
- [30] K.-J. Langenberg, R. Marklein, K. Mayer, *Ultrasonic Nondestructive Testing of Materials*, CRC Press, 2012
- [31] G. Dickson, *Ultrasonic methods for determination of mechanical properties of dental materials*, Gaithersburg, MD, 1969
- [32] B. Soufyane, F. Allou, M. Takarli, F. Dubois, N. Aurélie, Vers une détermination non destructive par ultrasons des propriétés mécaniques résiduelles des structures de chaussées, 24th Congrès Français de Mécanique, Brest, 2019

**Cite this article as:** Baraa Saidani, Jihed Zghal, Isabelle Bruant, Damien Bregiroux, Johann Petit, Julie Cedelle, Gaël Chevallier, Evaluation of mechanical properties of Ni/BaTiO<sub>3</sub> functionally graded material, *Mechanics & Industry* **25**, 10 (2024)